Toward Real-Time SQM for WAAS: Improved Detection Techniques

R. Eric Phelts, Todd Walter, Per Enge

Department of Aeronautics and Astronautics
Stanford University, Stanford, California

BIOGRAPHY

R. Eric Phelts is a Research Associate in the Department of Aeronautics and Astronautics at Stanford University. He received his B.S. in Mechanical Engineering from Georgia Institute of Technology in 1995, and his M.S. and Ph.D. in Mechanical Engineering from Stanford University in 1997 and 2001, respectively. His research involves multipath mitigation techniques and satellite signal anomalies.

Todd Walter received his B. S. in physics from Rensselaer Polytechnic Institute and his Ph.D. in 1993 from Stanford University. He is currently a Senior Research Engineer at Stanford University where his research focuses on algorithms that provide provable integrity for WAAS.

Per Enge is an Associate Professor of Aeronautics and Astronautics at Stanford University, where he has been on the faculty since 1992. His research deals with differential operation of GPS for landing aircraft. Previously, he was an Associate Professor of Electrical Engineering at Worchester Polytechnic Institute.

ABSTRACT

Signal Quality Monitoring (SQM) algorithms propose to detect anomalous signal distortions primarily through the use of SQM receivers. These receivers employ anywhere from three or more correlator pairs per channel—each slaved to the tracking pair. The measurements from each correlator output can be used to form detection metrics, which are, in general, simple algebraic combinations of the measurements. However, previously such metrics have been derived based primarily on observations of the correlation peak distortions or based on modeled characteristics of the measurement noise. This approach has traditionally led to a relatively large number of recommended detection metrics, and hence threshold tests. SQM2b (the suite of detection metrics validated for Cat I LAAS SQM), for example, calls for 11 tests.

For high-integrity applications, such as WAAS (and LAAS), large numbers of threshold tests pose several problems. The first is a continuity problem, since each test effectively poses an additional risk of false alarm. Another concern is the amount of energy and resources (i.e., manpower) required to validate the tests. For each, data must be collected, histograms must be analyzed, satisfactory overbounding must be performed for the integrity documentation. Given three SQM receivers at each of 25 WAAS reference stations, this could pose a significant workload. A third issue is one of efficiency and simplicity: fewer, more-effective tests should replace redundant and/or ineffective ones.

A more-efficient metric would combine the measurements from all correlators in a way that accounts for the anomalous signal distortion and that due to thermal noise and multipath. This paper describes an approach for formulating such metrics based on finding the eigenvectors of the signal-plus-noise system. It then introduces one such metric based on the measurements from an SQM receiver having a 16MHz bandwidth and Early-minus-Late correlator spacings of 0.05, 0.1, 0.15, 0.2 chips, respectively. (The tracking pair was the narrowest pair of 0.05 chips.) This paper assesses the performance of these tests in addition to several phenomenological or heuristic ones—including those analogous to the ones used to validate Cat I LAAS. In

addition, it provides and compares the alpha test specific to this SQM receivers, which is very similar to the ones expected for WAAS Offline Monitoring facilities.

INTRODUCTION

Signal Quality Monitoring (SQM) aims to prevent WAAS users from experiencing hazardously misleading information (HMI) caused by anomalous deformations of the GPS signal (i.e., so-called "evil waveforms"). High-integrity augmentation systems such as the Wide Area Augmentation System (WAAS) and the Local Area Augmentation System (LAAS) will employ multi-correlator receivers to this end. These receivers monitor the shape of the correlation function and detect any harmful signal deformations in the presence of noise and multipath.

WAAS was commissioned for Initial Operational Capability (IOC) in July of 2003. This first build offers full protection against the "Most Likely Subset"(MLS) signal deformation threat model, but it must equip its reference stations with SQM receivers and protect against all signal deformation threats to achieve compliance for FOC [9].

WAAS currently mitigates the MLS threat model using its Code-Carrier Coherence (CCC) Monitor. This monitor measures the rate of divergence between the code and carrier measurements on each satellite signal. The occurrence of hazardous MLS signal deformations causes this rate to exceed the detection threshold and cause the monitor to flag the SV as "Not Monitored."

Because of the pre-existing code-carrier divergence integrity threat, WAAS required no additional detection tests or monitors—beside the CCC monitor—to provide protection against the MLS signal deformation threats. The addition of true SQM receivers and accompanying multi-correlator processing techniques, however, will require that several additional threshold tests be performed to mitigate all deformation threats. (The International Civil Aviation Organization (ICAO) codified the full set of anomalous signal deformation threats to GPS in May 2000.) Accordingly, to date, the number of recommended SQM detection tests (e.g., for Cat I LAAS) has been relatively large [6].
However, in general, threshold tests are undesirable to add to an operational, high-integrity augmentation system. Each threshold test implemented increases the probability of false alarm and thereby hinders meeting stringent continuity requirements. Also, additional tests often require extensive validation in terms of noise and multipath performance. Since WAAS may have multiple SQM receivers at each of its (25 current) reference stations, the number of noise distributions to validate per threshold test may potentially become unmanageable. It may also be difficult to develop effective, non-redundant tests given uncertain receiver configurations or changing hardware requirements.

For all these reasons, it is preferable to have a reliable method for determining the minimal set of SQM detection metrics. (Note that a single detection metric is a mathematical combination of measurements. Each required metric corresponds to a single threshold/detection test.) This paper describes a straightforward and flexible, quantitative approach to computing a highly-effective detection metric, whose detection performance compares favorably to the use of numerous heuristically-derived metrics.

BACKGROUND

SV19

In 1993, a subtle failure occurred in the signal generating hardware aboard SV19. This failure went unnoticed for an extended period of time and was eventually resolved by the Control Segment. The OCS commanded the SV to switch to redundant signal generating hardware onboard the space vehicle. However, the anomaly persisted long enough to be observed and recorded by three different parties. [3]

The University of Leeds measured the power spectrum of PRN19 and observed a large spike at the center of the main lobe [1]. Trimble Navigation, Ltd. employed a local-area differential system using a reference receiver at 16MHz and 0.1 chips and a wide correlator at 4 observed 3-8 meter vertical (differential) position errors resulted whenever they included SV19 into the position solution. The Air Force base at Camp Parks, California used a high-gain antenna to record oscilloscope traces of the individual C/A code chips. They observed that the timing of the falling edge of this code had approximately a 33ns lag. In addition, those traces revealed increased oscillations indicative of analog "ringing" along each chip length.

ICAO Threat Model

The ICAO threat model was created by integrating the three observations of the original SV19 event. Although several other candidate threat models were considered, this model was the only one which was both realistic and able to create the three key correlation peak pathologies of concern to aviation users: false peaks, dead zones (or flat peaks), and distortions. [2]

In addition, this model is very tractable and relatively simple to analyze. It is formed by three parameters. The

lead/lag parameter, Δ (chips) models a digital failure by modifying the rising or falling edge of the C/A code—as observed by Camp Parks—and create dead zones atop the correlation peak. The two other parameters f_d and σ, model analog failures as 2nd-order "ringing"; in certain combinations these can create false peaks and correlation peak distortion.

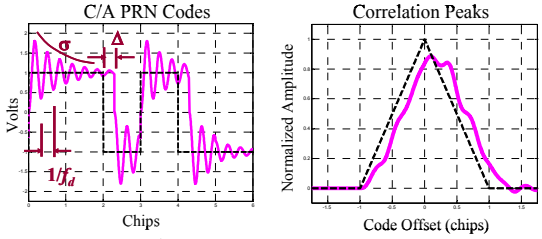

Figure 1. A "2nd-Order Step" anomalous waveform modeling both digital and analog failures and the corresponding correlation peak. (In this example, f_d =3MHz, σ= 0.8 MNepers/sec, Δ = 0.3chips)

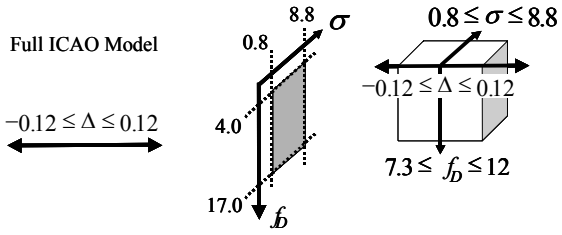

Figure 2. Parameter bounds for the full ICAO Threat Model

HEURISTIC DETECTION METRICS

Because Trimble Navigation, Ltd observed the original SV19 event using independent pseudorange differences, the first SQM detection metric designs envisioned on a number of independent pseudorange measurements taken from the same correlation peak. Such designs require SQM receivers to implement a number of independent tracking loops—each with a different correlator spacing—per receiver channel [3][8]. However, a more practical receiver implementation uses a single independent correlator spacing with additional (monitor) correlators arranged at fixed offsets relative to the tracking pair. This provides a single pseudorange measurement and a number of correlator values (i.e. correlation amplitude) measurements equal to the total number of correlator taps. Fortuitously, these amplitude measurements are actually more versatile in that they permit more mathematical measures, or metrics, of correlation peak symmetry to be formed than would simple pseudorange differences.

The first detection metrics leveraged experience and engineering judgment to formulate general rules, or heuristics, for determining the metrics most likely to detect the kinds of asymmetries likely to cause HMI. The two primary heuristics were:

- Independent pseudorange differences, which discovered the original SV19 event, should also be effective against significant ICAO threats
- Ratio measurements measured with respect to the peak should help detect dead zones or peak flattening effects

SQM2b

The first SQM detection metrics were proposed and analyzed jointly by AJ Systems, Honeywell, Raytheon, STNA, and Stanford University [5]. One candidate suite of metrics, termed "SQM2b," and was shown to meet the SQM performance for Category I LAAS installations using a total of three correlator pairs and a prompt measurement as depicted in Figure 2 below [6].

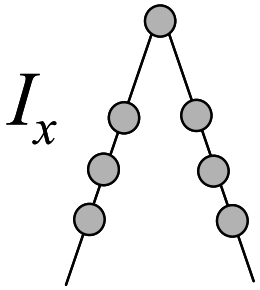

Figure 2. Illustration of a three-correlator pair SQM receiver configuration (with prompt measurement at peak). Each correlator output (I_x) is in-phase at a code offset, x, from the peak.

The correlator spacings—at code offsets, x—depicted in Figures 2-6 are (from left to right, in chips): [-0.1 -0.075 -0.05 0 +0.05 +0.75 +0.1]. The tracking pair is the narrowest pair at ±0.05 chips. Note that since the receiver is assumed to be phase-locked, only the in-phase measurements, I_x, are used for SQM. Using these seven correlator measurements, SQM2b formed the following 11 detection metrics (See Figure 3.):

- Two "Δ-metrics" (derived based on experiences with pseudorange differences):

$$\frac{\left(I_{-0.075}-I_{+0.075}\right)-\left(I_{-0.05}-I_{+0.05}\right)}{I_0},\quad \frac{\left(I_{-0.1}-I_{+0.1}\right)-\left(I_{-0.05}-I_{+0.05}\right)}{I_0} \tag{1}$$

- Three average ratio metrics:

$$\frac{I_{-0.05}-I_{+0.05}}{I_0},\ \frac{I_{-0.075}-I_{+0.075}}{I_0},\ \frac{I_{-0.1}-I_{+0.1}}{I_0} \tag{2}$$

- Six single-sided ratio metrics:

$$\frac{I_{-0.05}}{I_0}, \frac{I_{+0.05}}{I_0}, \frac{I_{-0.075}}{I_0}, \frac{I_{+0.075}}{I_0}, \frac{I_{-0.1}}{I_0}, \frac{I_{+0.1}}{I_0} \quad (3)$$

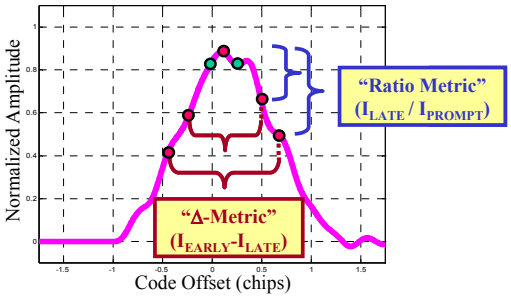

Figure 3. Generalized (heuristic) detection metrics for SQM2b.

Asymmetric Ratio Metrics

Intuitively, increasing the number of symmetry tests should increase the detection performance. Figure 4 illustrates how many more combinations of the correlator of the form $\frac{I_x}{I_y}$ or $\frac{I_x - I_y}{I_0}$ (for arbitrary code offsets, x and y) outputs may be used to form new metrics.

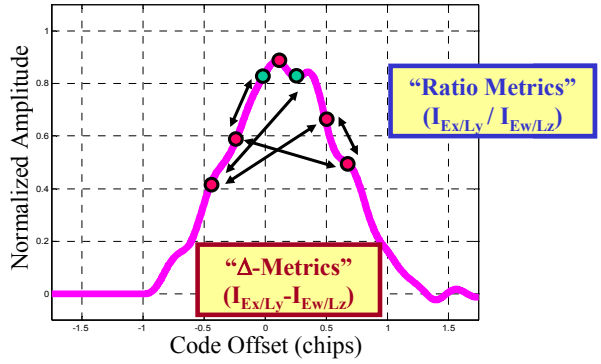

Figure 4. Several possible (asymmetric) ways to combine correlator measurements.

Polynomial Fit Metrics

A more sophisticated approach combines several correlator outputs to better mitigate the noise and multipath on each. Figure 5 illustrates two linear fits formed using the amplitudes and code offsets of the early and late sides of the correlation peak, respectively. From each fit, two line parameters (i.e., slope, ξ_1, and y-intercept, ξ_0) are found, and three amplitude estimates are given from the fit coefficients.

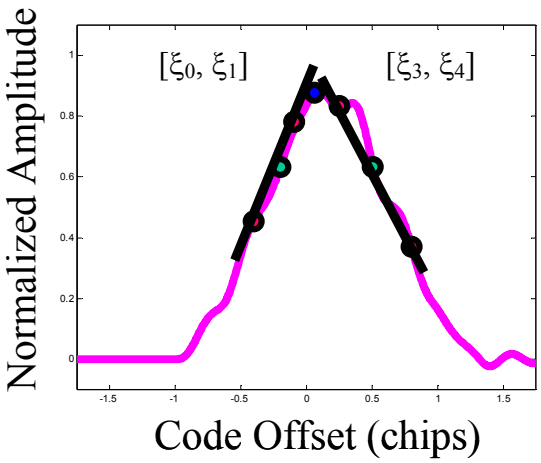

Figure 5. Two linear fits of correlator outputs (three early, three late). A total of ten parameters result from this fit: four line coefficients and six correlator measurement estimates.

More explicitly, for the aforementioned three-correlator pair SQM receiver, the linear fit metrics may be found from

- $\xi_0, \xi_1, \xi_3, \xi_4$
- $\hat{R}_{+0.05,P}$, $\hat{R}_{+0.075,P}$, $\hat{R}_{+0.1,P}$, $\hat{R}_{-0.05,P}$, $\hat{R}_{-0.075,P}$, $\hat{R}_{-0.1,P}$

where measured ratios $R_{x,P} = \frac{I_x}{I_0}$ and fit parameters ξ_0, ξ_1, ξ_3, ξ_4 are obtained by solving the folowing relation (using least-squares)

$$\begin{bmatrix} 0.05 & 1 \\ 0.075 & 1 \\ 0.1 & 1 \end{bmatrix} \begin{bmatrix} \xi_1 \\ \xi_0 \end{bmatrix} = \begin{bmatrix} R_{+0.05,P} \\ R_{+0.075,P} \\ R_{+0.1,P} \end{bmatrix} \quad (4)$$

and

$$\begin{bmatrix} -0.05 & 1 \\ -0.075 & 1 \\ -0.1 & 1 \end{bmatrix} \begin{bmatrix} \xi_3 \\ \xi_4 \end{bmatrix} = \begin{bmatrix} R_{-0.05,P} \\ R_{-0.075,P} \\ R_{-0.1,P} \end{bmatrix} \quad (5)$$

$\hat{R}_{+0.05,P}$, $\hat{R}_{+0.075,P}$, $\hat{R}_{+0.1,P}$, $\hat{R}_{-0.05,P}$, $\hat{R}_{-0.075,P}$, $\hat{R}_{-0.1,P}$ are smoothed estimates of the single-side ratios (the right-hand-side vectors in Equations 4 and 5 above). These are given by

$$\begin{bmatrix} \hat{R}_{+0.05,P} \\ \hat{R}_{+0.075,P} \\ \hat{R}_{+0.1,P} \end{bmatrix} = \begin{bmatrix} 0.05 & 1 \\ 0.075 & 1 \\ 0.1 & 1 \end{bmatrix} \begin{bmatrix} \xi_1 \\ \xi_0 \end{bmatrix} \quad (6)$$

and

$$\begin{bmatrix} \hat{R}_{+0.05,P} \\ \hat{R}_{+0.075,P} \\ \hat{R}_{+0.1,P} \end{bmatrix} = \begin{bmatrix} -0.05 & 1 \\ -0.075 & 1 \\ -0.1 & 1 \end{bmatrix} \begin{bmatrix} \xi_3 \\ \xi_4 \end{bmatrix} \quad (7)$$

Similarly, Figure 6 illustrates a single parabolic fit formed using the amplitudes and code offsets of both the early and late sides of the correlation peak (and the prompt measurement). From this second-order fit, three line parameters (i.e., c_0, c_1, and c_2) are found, and six amplitude estimates may be found from the fit coefficients. (Note that the prompt correlator must equal unity with or without any signal deformation present.)

9 parabolic fit metrics

- ξ_5, ξ_6, ξ_7
- $\breve{R}_{+0.05,P}$, $\breve{R}_{+0.075,P}$, $\breve{R}_{+0.1,P}$, $\breve{R}_{-0.05,P}$, $\breve{R}_{-0.075,P}$, $\breve{R}_{-0.1,P}$

ξ_5, ξ_6, ξ_7 are obtained by solving the folowing relation (using least-squares)

$$\begin{bmatrix} (0.1)^2 & -0.1 & 1 \\ (0.075)^2 & -0.075 & 1 \\ (0.05)^2 & -0.05 & 1 \\ 0 & 0 & 1 \\ (0.05)^2 & +0.05 & 1 \\ (0.075)^2 & +0.075 & 1 \\ (0.1)^2 & +0.1 & 1 \end{bmatrix} \begin{bmatrix} \xi_5 \\ \xi_6 \\ \xi_7 \end{bmatrix} = \begin{bmatrix} R_{-0.1,P} \\ R_{-0.075,P} \\ R_{-0.05,P} \\ 1 \\ R_{+0.05,P} \\ R_{+0.075,P} \\ R_{+0.1,P} \end{bmatrix} \quad (8)$$

$\breve{R}_{+0.05,P}$, $\breve{R}_{+0.075,P}$, $\breve{R}_{+0.1,P}$, $\breve{R}_{-0.05,P}$, $\breve{R}_{-0.075,P}$, $\breve{R}_{-0.1,P}$ are obtained are smoothed estimates of the single-side ratios (the right-hand-side vectors in Equation 9 below. These are given by

$$\begin{bmatrix} \breve{R}_{-0.1,P} \\ \breve{R}_{-0.075,P} \\ \breve{R}_{-0.05,P} \\ \breve{R}_{+0.05,P} \\ \breve{R}_{+0.075,P} \\ \breve{R}_{+0.1,P} \end{bmatrix} = \begin{bmatrix} (0.1)^2 & -0.1 & 1 \\ (0.075)^2 & -0.075 & 1 \\ (0.05)^2 & -0.05 & 1 \\ (0.05)^2 & +0.05 & 1 \\ (0.075)^2 & +0.075 & 1 \\ (0.1)^2 & +0.1 & 1 \end{bmatrix} \begin{bmatrix} \xi_5 \\ \xi_6 \\ \xi_7 \end{bmatrix} \quad (9)$$

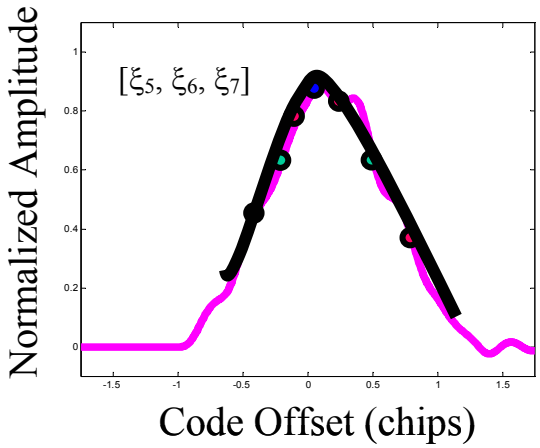

Figure 6. A single parabolic fit of all seven correlator outputs. A total of nine parameters result from this fit: three second-order fit coefficients and six correlator measurement estimates.

The next section derives a metric design approach which meets addresses all of these considerations.

ALPHA METRIC

Since the heuristic approach to SQM detection metric design has no strict definition of success or performance, it is likely to result an unacceptably large number of metrics (and, hence, threshold tests), a more quantitative approach is needed. It follows that a reasonable quantitative method designed to minimize the number of SQM detection tests required for WAAS and to maximize their effectiveness requires three key considerations:

1) Use all available correlators: The metric should optimize performance by using all available measurements.
2) Make use of all *a priori* information: The metric should incorporate knowledge of the ICAO threat model and the noise and multipath effects on each correlator measurement
3) Perform all complex computations offline: Any complex computations should only be done in the design stage. The resulting metric should form a simple linear combination of the correlator outputs to best maintain any

assumptions on Gaussian nature of the resulting noise statistics.

4) Support straightforward redesign for arbitrary SQM receiver configurations.

Derivation

To ensure detection, for a single (in-phase) correlation peak measurement, the distorted waveform value (I_{ewf}) must exceed the nominal correlation peak (I_{ref}) value by a function of the noise and the detection metric. Equation xx1 below gives this expression for the case where the metric is a simple scalar multiple, α, of the in-phase correlator measurements, I.

$$I_{ewf}\alpha \geq I_{ref}\alpha + \left| f(\sigma_{test}, \alpha) \right| \quad (10)$$

Minimum Detectable Errors (MDEs) define the minimum detection threshold (i.e., the deviation from nominal) required by a specific detection metric to meet the requirements on probability of false alarm (P_{fa}) and probability of missed detection (P_{md}). In general, we do not know the MDE without knowing the nature of nominal measurement conditions transformed by the detection metric. For gaussian noise models of thermal noise and multipath, P_{fa} and P_{md} yield scalar multiples of the metric standard deviation, σ_{test}. These are k_{ffd} and k_{md}, respectively.

The effect of the metric on the nominal noise variance can be conservatively assumed as a product of multiple of the metric itself, $\lambda\alpha$. Note that this simple assumption may always be considered conservative for sufficiently large, positive number, λ.) This expression is given below in Equation 11 (where the absolute value has been ignored for now).

$$I_{ewf}\alpha \geq I_{ref}\alpha + \left[\sigma_{test}(k_{ffd} + k_{md})\right] \cdot \lambda\alpha \quad (11)$$

This may be extended for a matrix of correlation peak deformation responses, I_{ewf}, as given in equation xx3.

$$\mathrm{I}_{ewf}\overline{\alpha} \geq \mathrm{I}_{ref}\overline{\alpha} + \left(\Sigma_{test}k_{tot}\right)\Lambda\overline{\alpha} \quad (12)$$

where

I_{ref} is the corresponding nominal, in-phase correlation measurement matrix,

Σ_{test} is the matrix of standard deviations,

k_{tot} is the sum of noise multipliers, k_{ffd} and k_{md},

Λ is a diagonal matrix of scalar multipliers

$\overline{\alpha}$ is the vector of constants multiplying each correlation measurements

By recognizing that the distortions from nominal are given by

$$\mathrm{I}_{e-r} = \mathrm{I}_{ewf} - \mathrm{I}_{ref}, \quad (13)$$

Equation 12 can be re-written as

$$\mathrm{I}_{e-r}\overline{\alpha} \geq \left(\Sigma_{test}k_{tot}\Lambda\right)\overline{\alpha} \quad (14)$$

Equation 14 can be solved as an eigenvalue problem for a matrix of eigenvectors, **A**, by taking the pseudoinverse of matrix quantity $\Sigma_{test}k_{tot}$ according to Equation 15.

$$\left(\Sigma_{test}k_{tot}\right)^{\dagger}\mathrm{I}_{e-r}\overline{\alpha} \geq \Lambda\overline{\alpha} \quad (15)$$

Practical Considerations

To prioritize more harmful threats over less-harmful ones, each row of $\Sigma_{test}k_{tot}$ should be divided by the pseudorange error corresponding to that threat (row). (These maximum range errors are easily-obtainable for typical Early-minus-Late or $\Delta\Delta$ user receiver configurations through the analysis given in [5] and [6].) Note, however that the matrix $\left(\Sigma_{test}k_{tot}\right)$ may be poorly-conditioned under some circumstances (e.g., extremely small standard deviations on all correlator pairs). For this reason, it may be helpful to condition the matrix prior to inversion. This can be done by pre-multiplying the quantity each side of Equation 14 by a known matrix **A** as shown in Equation 16.

$$\mathrm{A}\mathrm{I}_{e-r}\overline{\alpha} \geq \left(\mathrm{A}\Sigma_{test}k_{tot}\right)\Lambda\overline{\alpha} \quad (16)$$

Although the best possible matrix **A** has not yet been formulated, Equations 17 through 19 list three candidates which have been shown to yield good results.

$\mathrm{A} = \mathrm{I}_{ref}^{\mathrm{T}}$:

$$\left(\mathrm{I}_{ref}^{\mathrm{T}}\Sigma_{test}k_{tot}\right)^{\dagger}\mathrm{I}_{ref}^{\mathrm{T}}\mathrm{I}_{e-r}\overline{\alpha} \geq \Lambda\overline{\alpha} \quad (17)$$

$\mathrm{A} = \mathrm{I}_{ewf}^{\mathrm{T}}$:

$$\left(\mathrm{I}_{ewf}^{\mathrm{T}}\Sigma_{test}k_{tot}\right)^{\dagger}\mathrm{I}_{ewf}^{\mathrm{T}}\mathrm{I}_{e-r}\overline{\alpha} \geq \Lambda\overline{\alpha} \quad (18)$$

$\mathrm{A} = \mathrm{I}_{e-r}^{\mathrm{T}}$:

$$\left(\mathrm{I}_{e-r}^{\mathrm{T}}\Sigma_{test}k_{tot}\right)^{\dagger}\mathrm{I}_{e-r}^{\mathrm{T}}\mathrm{I}_{e-r}\overline{\alpha} \geq \Lambda\overline{\alpha} \quad (19)$$

The alpha metric will be the real eigenvector $\overline{\alpha}$ that best mitigates the distortion threats contained in the matrix, $\mathbf{I}_{ewf}$. It will correspond to the non-zero eigenvalue, λ_{ii}.

ANALYSIS AND RESULTS

The SQM receiver configuration used to evaluate the alpha metric was a 4-correlator pair receiver with spacings—at code offsets, x—(from left-to-right, in chips) [-0.1 -0.075 -0.05 -0.025 +0.025 +0.05 +0.75 +0.1]. The tracking pair used the correlators at offsets x=±0.025chips. (See Figure 7.)

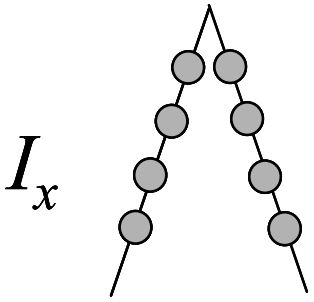

Figure 7. Eight correlator pair SQM receiver configuration. I_x refers to each (in-phase) correlator output at code offset x with respect to the ideal peak (at x=0).

Nominal Noise and Multipath Measurements

The thermal noise and multipath effects on each correlator measurement were measured using one of the rooftop antennas of the LAAS Integrity Monitoring Testbed at Stanford University [7]. The data uses four complete passes from SV5. Figure 8 plots the standard deviations measured (x1000) at each correlator output. (Note that the correlator measurements have been normalized by the average of the tracking pair at x=±0.025chips.)

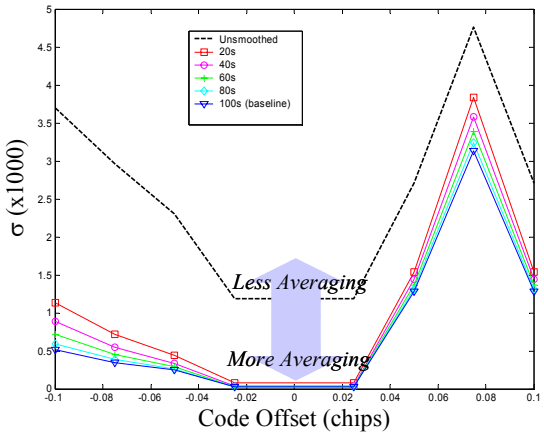

Figure 8. Standard deviations of noise and multipath on correlator measurements. The measurements correspond to SV5 at a 5° elevation angle.

As expected, the smallest standard deviation occurs for the tracking pair—which was used to normalized the others. There is also significantly less distortion on the left half of the correlation peak than on the right. This is due to the fact that multipath affects the late side of the correlation peak much more than it does the early side. In fact, the largest standard deviation occurs at code offset x=+0.075chips, which indicates the presence of a significant multipath reflection at approximately this delay from the line-of-sight signal. Of course, since multipath is site-dependent, this particular correlator-noise distribution will not apply in general.

The figure also shows the effects of smoothing on the standard deviation. The uppermost line corresponds to unsmoothed data, while the lowermost corresponds to a 100-second moving average. Although much of the benefit is appears to be achieved after the first 20-second filter is applied, less than 100 seconds of averaging is seldom sufficient for good SQM performance. Also, since 100 seconds has been a standard for SQM analyses in the past, subsequent analyses used 100-second filter noise levels [6].

Minimum Detectable Error (MDE)

The minimum detectable errors (MDEs) define the detection threshold limits required to guarantee detection of the signal deformation with the specified probability of missed detection (P_{md}) and false alarm probability (P_{fa}). For Phase I WAAS, the current fault tree allocation for SV19-like failures is 10^{-10} per approach and requires a P_{fa} of 3.2×10^{-8} false alarms per satellite per second (for all approach cases). This corresponds to a constant standard deviation multiplier, k_{ffd}, of 5.54.

The accompanying P_{md} is found from the fault tree integrity risk (i.e., P_{HMI}) allocations and a priori satellite failure rate probabilities. The P_{HMI} allocations for this monitor from the current WAAS fault tree and the GPS SV-19 threats is 8.333e-10 per approach. For an *a priori* failure probability, $P_{f\_apriori}$ =1e-4, the P_{md} requirement for GPS SV-19 failures is 8.33e-6. This corresponds to a k_{md} of 4.46. [9]. Accordingly, for this analysis, $k_{tot} = k_{md}+k_{ffd}$ = 10. (Note that for the analyses in this paper, the standard deviations have not been Gaussian overbounded.)

Threat Model Discretization

To analyze SQM performance—using either heuristically or more deterministically-derived methods—the three-dimensional ICAO threat space must be discretized with a resolution sufficient to capture all significant threats [4][5]. Accordingly, for each parameter, the following discretizations were chosen:

Δ: varied from 0 to 0.12chips in increments of 0.01chips. (See Figure 9.)

σ: varied from 0.8 to 8.8MNepers/sec in increments of 0.5MNepers/sec.
f_d: varied from 4 to 17MHz (for the analog failure mode) and 7.3 to 13MHz in increments of 0.1MHz.

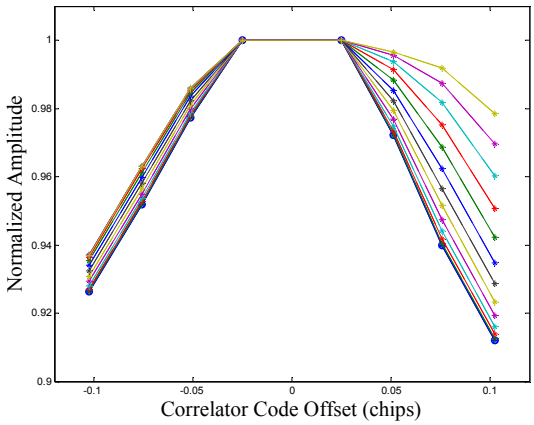

Figure 9. Eight correlator outputs for the reference (nominal) correlation function and the 13 discretized lead/lag (Δ) deformation threats—including Δ=0.

Example: Two Signal Deformation Case

Consider the case of only two deformations: one digital-only failure (Δ = 0.12 chips, f_d = 0MHz) and one purely analog (f_d = 4MHz, σ = 0.8MNepers/sec, and Δ = 0 chips). Assuming a normalized (model) correlation peak filtered at 16MHz using a 6th-order Buttterworth filter model, for the 8-correlator SQM receiver configuration depicted in Figure 7, the alpha metric may be formulated according to Equation 15.

The nominal correlation matrix ($\mathbf{I}_{ref}$), the deformed correlation matrix ($\mathbf{I}_{ewf}$) and the MDE matrix ($\Sigma_{test}k_{tot}$) are each given by.

$$\mathbf{I}_{ref} = \begin{bmatrix} 0.9263 & 0.9519 & 0.9774 & 1.0000 & 1.0000 & 0.9722 & 0.9398 & 0.9121 \\ 0.9263 & 0.9519 & 0.9774 & 1.0000 & 1.0000 & 0.9722 & 0.9398 & 0.9121 \end{bmatrix}$$

$$\mathbf{I}_{ewf} = \begin{bmatrix} 0.9368 & 0.9630 & 0.9860 & 1.0000 & 1.0000 & 0.9966 & 0.9918 & 0.9784 \\ 0.9455 & 0.9698 & 0.9875 & 1.0000 & 1.0000 & 0.9744 & 0.9283 & 0.8695 \end{bmatrix}$$

$$\Sigma k_{tot} = \begin{bmatrix} 5.11e-2 & 3.41e-2 & 2.47e-2 & 1.43e-4 & 1.43e-4 & 1.27e-1 & 3.12e-1 & 1..27e-1 \\ 5.58e-2 & 3.73e-2 & 2.70e-2 & 1.43e-4 & 1.43e-4 & 1.39e-1 & 3.41e-1 & 1.39e-1 \end{bmatrix}$$

Note that the rows of $\Sigma_{test}k_{tot}$ have been scaled by each deformation's maximum range errors—for Early-minus-Late user receivers—of 0.0665 chips (19.5m) and 0.0607 chips (17.8m), respectively. (The virtual prompt values (i.e., 1.43e-4) have remained unscaled, however.)

Here, the MDEs correspond to a 5° elevation angle and assume 5 WREs are available to average the noise. (These are minimum acceptance criteria for WAAS satellites.) The net deformation matrix ($\mathbf{I}_{e\text{-}r}$) simply subtracts $\mathbf{I}_{ref}$ from $\mathbf{I}_{ewf}$ and is given by

$$\mathbf{I}_{e\text{-}r} = \begin{bmatrix} 0.0105 & 0.0111 & 0.0086 & 1.0000 & 1.0000 & 0.0244 & 0.0519 & 0.0663 \\ 0.0192 & 0.0179 & 0.0101 & 1.0000 & 1.0000 & 0.0022 & -0.0116 & -0.0425 \end{bmatrix}$$

The non-zero eigenvalues (i.e., $|\lambda|>\varepsilon>0$) of Equation EE, will select the valid alpha metric candidates for all four of the candidate A matrices.

The metric solutions are given below in Equation 21. Note that in all the results that follow, the eigenvalues (λ) and corresponding eigenvectors/alpha metrics ($\overline{\alpha}$) have two subscript identifiers. The first indicates to which of Equations 16-19 (numbered 1-4, respectively) they correspond. The second subscript indicates number of the eigenvalue (i.e., the matrix column) selected within each respective solution. (For succinctness, only the eigenvectors corresponding to Equation 17 are given in Equation 20.)

$$\begin{aligned} &\left\{\lambda_{2,3} \middle| \geq \varepsilon : 0.0783\right\} \\ &\left\{\lambda_{2,4} \middle| \geq \varepsilon : 6.94x10^{-18}\right\} \\ &\left\{\lambda_{2,5} \middle| \geq \varepsilon : 1.47x10^{-18}\right\} \\ &\left\{\lambda_{2,8} \middle| \geq \varepsilon : 8.37x10^{-20}\right\} \end{aligned} \tag{20}$$

$$\overline{\alpha}_{2,5} = \overline{\alpha}_{best} = \begin{bmatrix} -0.2834 \\ -0.3752 \\ -0.1891 \\ -0.0013 \\ -0.0002 \\ 0.4197 \\ -0.1471 \\ 0.7385 \end{bmatrix} \tag{21}$$

Figure 10 best shows the effectiveness of this alpha metric. The product of the metric with the reference correlation measurements yields a nominal value of approximately 1.75. (The units are dimensionless.) The corresponding MDE—specific to the alpha metric—brackets a range of values between which no deformations are detectable. However, the product of the alpha metric with the deformation matrix ($\mathbf{I}_{ewf}$) causes the two deformations to fall well outside of this region. This indicates the alpha metric can detect these deformations. In fact, they are detectable with margin.

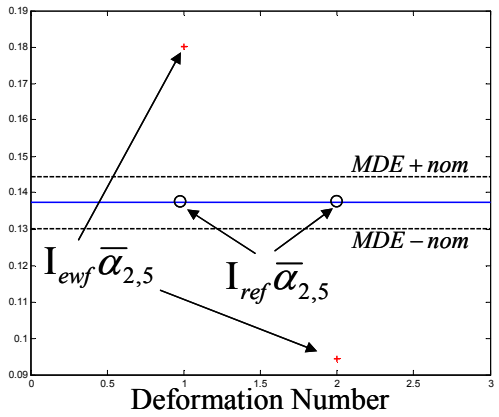

Figure 10. Alpha metric detectability plot of two signal deformations for the "best" eigenvector solution. Deformations 1 and 2 correspond to the digital failure mode and analog failure mode, respectively.

The second-best alpha metric in this example also detects both deformations. However, it does so with slightly smaller margin. (See Figure 11.) As did the previous metric, this one also results from Equation 17.

$$\overline{\alpha}_{2,8} = \begin{bmatrix} 0.6994 \\ -0.5804 \\ -0.1328 \\ -0.0263 \\ -0.0088 \\ -0.2146 \\ 0.2410 \\ -0.2268 \end{bmatrix} \tag{22}$$

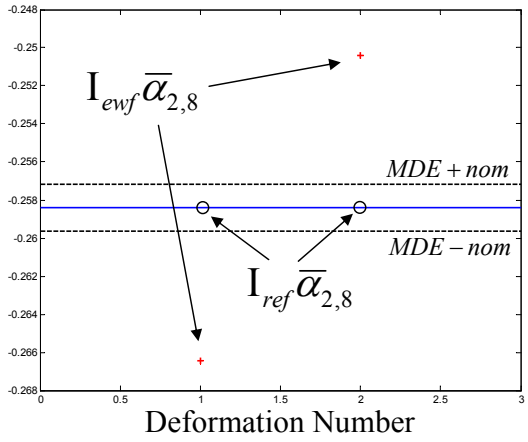

Figure 11. Alpha metric detectability plot of two signal deformations for the second-best eigenvector solution. Deformations 1 and 2 correspond to the digital failure mode and analog failure mode, respectively.

Two primary observations can be made from this example. First, the precise values of the eigenvalues are relatively unimportant. Instead, the effectiveness of each alpha metric is of key concern. Second, the value of the nominal product $I_{ref}\overline{\alpha}$ is also relatively unimportant. Of significantly more importance is the range of values about $I_{ref}\overline{\alpha}$ bracketed by the alpha metric MDE. A narrower "undetectable" range implies better effective noise averaging by the metric.

Example: Full ICAO Threat Model

The discretized ICAO threat model consists of 15058 deformation threats (including the one zero-deformation or nominal case), but the basic formulation of the problem remains the same. However, for the same receiver configuration, $\mathbf{I}_{ewf}$ now has 15058 rows and 8 columns; $\mathbf{I}_{ref}$, $\Sigma_{test}k_{tot}$, and $\mathbf{I}_{e\text{-}r}$ have the same dimensions. Metric selection (i.e., from the eigenvalues with magnitudes greater than 10^{-20}) is the same as in the two-deformation case.

The "best" alpha metric is given below. In addition, the second-best candidate metric ($\overline{\alpha}_{2,1}$) is shown. This alpha metric evaluation is shown in Figure 12. It detects all but 840 of 15057 ICAO deformation threats (i.e., excluding the nominal, non-deformed case). The second-best metric, $\overline{\alpha}_{2,1}$, leaves 4943 threats undetected.

$$\overline{\alpha}_{3,2} = \overline{\alpha}_{best} = \begin{bmatrix} 0.0432 \\ 0.0614 \\ -0.0456 \\ -0.0004 \\ 0.0004 \\ -0.6135 \\ 0.4895 \\ -0.6134 \end{bmatrix} \tag{23}$$

$$\overline{\alpha}_{2,1} = \begin{bmatrix} -0.2079 \\ -0.0671 \\ -0.0713 \\ 0.0013 \\ 0.0020 \\ -0.6398 \\ -0.3680 \\ -0.6344 \end{bmatrix} \tag{24}$$

Recall that in the two-deformation case, all the candidate solutions were the same for each alpha metric equation. Also, there was only a single candidate metric (solution)

for each equation. Conversely, in this case, there are 15 candidate alpha-metrics—only two of which are identical. It is only by evaluating the product $I_{ewf}\overline{\alpha}$ (as illustrated in Figure 12) that the best metric—the one which detects the most deformations—can be determined.

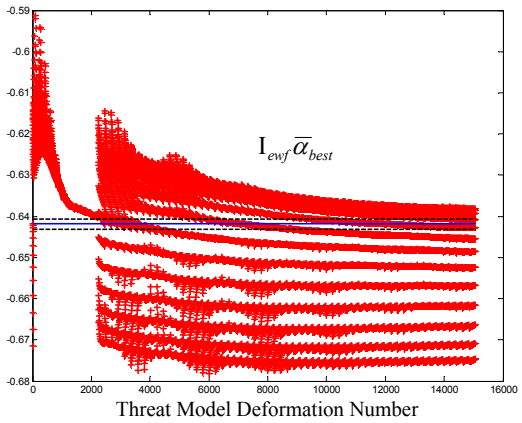

Figure 12. Alpha metric detectability plot of all ICAO signal deformation threats.

Figures 13 and 14 illustrate the noise averaging capability of the alpha metric. Figure 13 shows the standard deviation of the undetectable deformations compared against the MDEs on each correlator output. The uppermost (red) curve shows the MDE for a single receiver. The middle (blue) curve depicts the standard deviation of all the ICAO deformations versus correlator offset. The third (red) curve shows the results for the same receiver reduced by $\sqrt{5}$ (i.e., averaged by 5 WAAS SQM receivers). Figure 14 shows the same two MDE curves compared against the standard deviation of the 840 deformations remaining after application of the alpha metric. Note that these variations are well below the MDEs on each correlator output. This indicates that detecting these remaining deformations is significantly more difficult.

Figure 15 compares the user differential pseudorange errors remaining after applying the alpha metric to those remaining after applying the most effective of 56 heuristic metrics of the type described previously. (For the eight-correlator pair configuration, the heuristic tests included six delta metrics, 27 ratios and 23 curve fit—both linear and parabolic—metrics.) However, only four of the 56 heuristic tests are actually required; others are either redundant or detect no ICAO deformations at all. Interestingly, the most effective heuristic test—for this receiver configuration and multipath environment—comes from one of the parabolic fit estimates of the correlator location. For these MDEs (and this receiver configuration), it detects even more (737 of 15057) deformation threats than does the alpha metric.

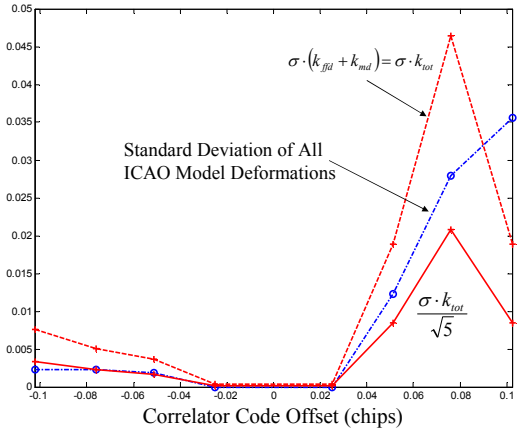

Figure 13. Comparison of *pre-detection* deformation standard deviation to correlation noise measurement variations. The MDE measurements (in red) correspond to a 5° elevation angle

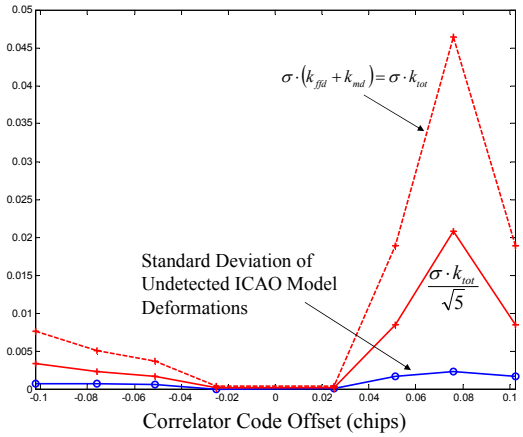

Figure 14. Comparison of *post-detection* deformation standard deviation to correlation noise measurement variations. The MDE measurements (in red) correspond to a 5° elevation angle.

The plot also shows that the alpha metric actually produces somewhat smaller (albeit comparable) maximum user range errors—despite detecting fewer total threats than the best heuristic test. This seeming contradiction arises from the fact that the threats most difficult to detect tend to cause relatively small (but comparable) user range errors. In this case, the alpha metric detects a few that actually are slightly more harmful to the user than those detected by the best heuristic metric. Recall that this occurs by design since the maximum range errors for each threat are used to scale the detection thresholds in the alpha metric formulation.

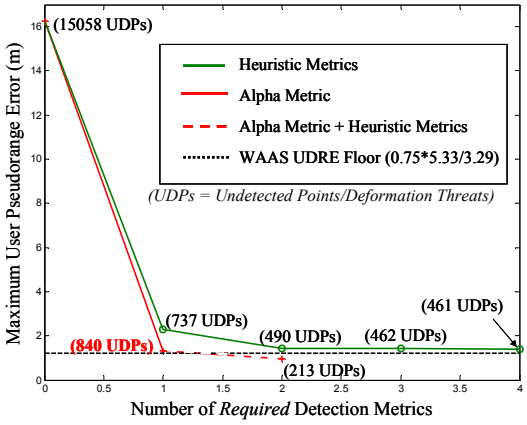

Figure 15. Maximum user pseudorange error comparison of effectiveness of the alpha metric (red) to all required heuristic metrics (green). The number of undetected deformations after the application of each metric is provided in parentheses above each respective metric index.

It follows that the combination of the best heuristic metric and the alpha metric detects the largest number of threats and leaves the smallest user range errors. As shown in Figure 15, this combination leaves only 213 threats undetected and results in a maximum user error below the smallest UDRE WAAS can provide. (Figure 16 shows which portion of the ICAO threat space these remaining deformations occupy.) No other heuristic metrics improve the detection capability beyond this. Still, were this SQM receiver configuration (and these noise and multipath levels) valid for WAAS, only two detection/threshold tests would nominally satisfy the all future (steady-state) SQM performance requirements [9].

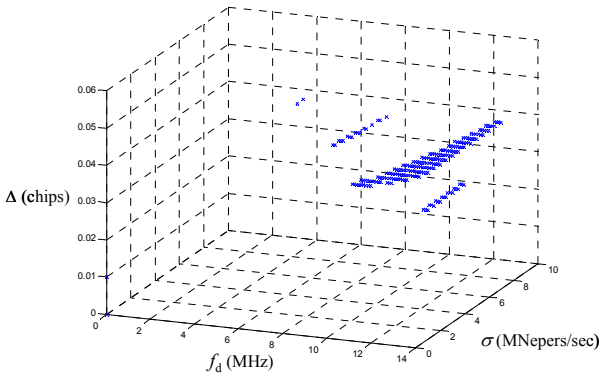

Figure 16. Locations of 213 remaining deformations within the ICAO threat space after application of alpha metric and the best heuristic detection metric.

CONCLUSIONS

The alpha metric is a simple linear combination of correlator measurements derived based on a known receiver configuration and given the noise measurements on each correlator output. Conventional, heuristic approaches do not rely on this information in their design. As a result many metrics (and, hence, threshold tests) are needed to assure satisfactory SQM performance under a variety of antenna siting and environmental conditions. Numerous threshold tests are undesirable since they imply an increase in false alarm probability and algorithm complexity.

A single alpha metric together with the best heuristic metrics may be the most efficient way to achieve satisfactory SQM performance with the least number of tests. Accordingly, the two primary advantages of implementing the alpha metric are as follows:

1) It can significantly reduce the total number of tests required to meet the SQM performance requirements.
2) It provides a straightforward method to redesign based on an arbitrary SQM receiver configuration and/or multipath environment.

REFERENCES

[1] Daly, P., Riley, S., Raby, P. "Recent Advances in the Implementation of GNSS," *Proceedings of the 6th International Technical Meeting of the Satellite Division of the Institute of Navigation*, ION-GPS 1993, September 1993, pp. 433-40.

[2] Enge, P. K., Phelts, R. E., Mitelman, A. M., "Detecting Anomalous signals from GPS Satellites," ICAO, GNSS/P, Toulouse, France, 1999.

[3] Edgar, C., Czopek, F., Barker, B., "A Co-operative Anomaly Resolution on PRN-19," *Proceedings of the 2000 13th International Technical Meeting of the Satellite Division of the Institute of Navigation, ION GPS-2000*. Proceedings of ION GPS 2000, v 2, pp. 2269-271.

[4] Macabiau, C., Chatre, E., "Impact of Evil Waveforms on GBAS Performance," *Position Location and Navigation Symposium*, IEEE PLANS, 2000, pp. 22-9.

[5] Phelts, R. E. "Multicorrelator Techniques for Robust Mitigation of Threats to GPS Signal Quality," Ph.D. Thesis, Stanford University, Stanford, CA, 2001.

[6] Phelts, R. E., Akos, D. M., Enge, P. K., "Robust Signal Quality Monitoring and Detection of Evil Waveforms," *Proceedings of the 13th International Technical Meeting of the Satellite Division of the Institute of Navigation*, ION-GPS-2000, pp. 1180-90.

[7] Pullem, S., Luo, M., Gleason, S., Xie, G., Lee, J., Akos, D., Enge, P., Pervan, B., "GBAS Validation

Methodology and Test Results from the Stanford LAAS Integrity Monitor Testbed," *Proceedings of the 13th International Technical Meeting of the Satellite Division of the Institute of Navigation*, ION-GPS-2000, pp. 1191-201.

[8] Shively, C., Brenner, M., Kline, P., "Multiple Ground Tests Protecting Against Satellite Correlation Symmetry Faults in LAAS," (Revision 3), RTCA SC-159, 1999.

[9] Shloss, P., Phelts, R. E., Walter, T., Enge, P. K., "A Simple Method of Signal Quality Monitoring for WAAS LNAV/VNAV," *Proceedings of the 15th International Technical Meeting of the Satellite Division of the Institute of Navigation*, ION-GPS-2002, pp. 800-8.